

Atomistic simulations of ½ screw dislocation core in magnesium oxide

Philippe Carrez, Julien Godet, Patrick Cordier

▶ **To cite this version:**

Philippe Carrez, Julien Godet, Patrick Cordier. Atomistic simulations of ½ screw dislocation core in magnesium oxide. Computational Materials Science, 2015, Computational Materials Science, 103, pp.250-255. 10.1016/j.commatsci.2014.10.019 . hal-02545016

HAL Id: hal-02545016
https://hal.univ-lille.fr/hal-02545016

Submitted on 16 Apr 2020

HAL is a multi-disciplinary open access archive for the deposit and dissemination of scientific research documents, whether they are published or not. The documents may come from teaching and research institutions in France or abroad, or from public or private research centers.

L'archive ouverte pluridisciplinaire **HAL**, est destinée au dépôt et à la diffusion de documents scientifiques de niveau recherche, publiés ou non, émanant des établissements d'enseignement et de recherche français ou étrangers, des laboratoires publics ou privés.



Distributed under a Creative Commons Attribution - NonCommercial - NoDerivatives 4.0 International License

Computational Materials Science 103 (2015) 250–255

Contents lists available at ScienceDirect

Computational Materials Science

journal homepage: www.elsevier.com/locate/commatsci

Atomistic simulations of ½⟨1 1 0⟩ screw dislocation core in magnesium oxide

Ph. Carrez [a,*], J. Godet [b], P. Cordier [a]

[a] Unité Matériaux et Transformations, Université de Lille1, UMR CNRS 8207, 59655 Villeneuve d'Ascq cedex, France
[b] Institut Pprime, Dept PMM, CNRS-UPR 3346, Université de Poitiers, 86962 Futuroscope Chasseneuil, France

ARTICLE INFO

Article history:
Received 25 June 2014
Received in revised form 30 September 2014
Accepted 10 October 2014
Available online 6 November 2014

Keywords:
Dislocation
Core spreading
Core energy
High pressure

ABSTRACT

Atomistic calculations of the ½⟨1 1 0⟩ screw dislocation core structure in MgO have been carried out showing the influence of high pressure (up to 100 GPa) on the core spreading. Calculations rely on a periodic arrangement of dislocation quadrupoles. Comparison between first principles and pairwise potential simulations show a remarkable agreement. Our results confirm that the dislocation core evolves from a spreading in {1 1 0} (at low pressure) to a narrower configuration spread in {1 0 0} as pressure increases. The periodic dipole method enables us also to record the pressure induced core energy variations.

© 2014 The Authors. Published by Elsevier B.V. This is an open access article under the CC BY-NC-ND license (http://creativecommons.org/licenses/by-nc-nd/3.0/).

1. Introduction

The dislocations core structure at the atomic scale is nowadays accessible in numerical modelling. Generally based on empirical potentials calculations [1–7], recent advances have been made to study the atomistic configurations around the dislocation core through First-Principles calculations (*e.g.* [8,9]). However the long-range displacement field of a dislocation requires large-scale simulations unachievable by this technique. To overcome this numerical limitation, a periodic arrangement of dipole or quadrupole of dislocations can be used to cancel the displacement field at large distance [10]. Such periodic calculations have been intensively used to study dislocation core structure in metals [11–14] or in semiconductors [15,16]. Despite the importance of dislocation core structure in materials such as ionic crystals, calculations of dislocation core structure based on periodic arrangement of array of dislocations have never been undertaken in ionic materials. Indeed, most of atomistic analysis of dislocation core structures have been performed using large scale simulations involving empirical potentials [17–25]. In magnesium oxide (MgO), Woo and co-workers have intensively studied the edge dislocation with ½⟨1 1 0⟩ Burgers vector [17–20]. More recently, studies of screw dislocation cores have been achieved [20–24,26] involving ⟨1 0 0⟩ or ½⟨1 1 0⟩ Burgers vectors. Until now, the atomistic studies of the screw dislocation with a ½⟨1 1 0⟩ Burgers vector have never been focussed on the detailed core structure, known to be the important parameter controlling the mobility of dislocations [27].

On the other hand, recent modelling of core structures based on the continuum Peierls–Nabarro (PN) model [28–30] have revealed the potential influence of pressure on the screw dislocation core in MgO. However, conclusions arising from continuum modelling may always be subjected to the inherent assumptions of the PN model. The purpose of this study is therefore to revisit current knowledge of dislocation core structure in MgO based on both empirical potential calculations and Density Functional Theory (DFT) calculations using periodic quadrupolar arrangement of dislocations. Here, we focus on the ½⟨1 1 0⟩ screw dislocation in MgO and the evolution of its core structure under increasing pressure. For comparison purpose, we will consider the following pressure, 0, 30, 60 and 100 GPa, falling in the pressure range of the Earth mantle as investigated in a previous work [30].

2. Methods and simulation cells

All calculations have been performed using a periodically quadrupolar arrangement of four ½⟨1 1 0⟩ screw dislocations. The choice of periodic boundary conditions associated with a quadrupolar arrangement was driven by the necessity to minimize residual strains within simulations cells [31]. The cell orientation corresponds to a crystal with [0 0 1] oriented along *x*, [1 −1 0] along *y*, and [1 1 0] (considered in the following as the direction of the

* Corresponding author.
E-mail address: philippe.carrez@univ-lille1.fr (Ph. Carrez).

http://dx.doi.org/10.1016/j.commatsci.2014.10.019
0927-0256/© 2014 The Authors. Published by Elsevier B.V.
This is an open access article under the CC BY-NC-ND license (http://creativecommons.org/licenses/by-nc-nd/3.0/).

Burgers vector) along z. The basic block (Fig. 1) was chosen to correspond to $2a \times a\sqrt{2}/2 \times b$ (where a corresponds to the lattice parameter of the structure and b to the magnitude of the Burgers vector of $\frac{1}{2}\langle 1\,1\,0\rangle$ dislocation), the cell dimensions were further increased by multiplying the initial block by an integer n along x and y in order to keep a constant ratio $x/y = 2\sqrt{2}$. The smallest volume used ($36a^3$) is therefore based on $n = 6$, containing 288 atoms whereas the largest system size is simulated for $n = 80$ (51,200 atoms in a $6400a^3$ volume). Depending on the actual spreading of the core, all system sizes could not be considered at every pressure. A typical $n = 8$ value (*i.e.* a quadrupolar arrangement inside a system of 512 atoms) was considered for DFT calculations. The initial four dislocations were then introduced by applying the displacement field of a quadrupole of dislocations, as given by the linear isotropic elasticity, on the atomic position of the pristine system (see [32] for practical implementation details). The energy minimization for all systems were further performed at fixed volume, *i.e.* the lattice parameter a was rescaled to equilibrium values corresponding to each pressure (Table 1).

Using such atomic configuration, the energy of a straight dislocation line of Burgers vector b is given by Eq. (1), resulting from a regularization of the infinite sum of logarithm terms involved in the interaction energy between pairs of dislocations [11,15]:

$$E = E(r_c) + \frac{\mu b^3}{4\pi}\{Ln(d_1/r_c) + A(d_1/d_2)\} \quad (1)$$

where r_c correspond to a given cut-of radius for the core energy; d_1 and d_2 correspond to the equilibrium distances between positive and negative dislocation along the x and y directions and $A(d_1/d_2)$ a function containing all dislocations pair-wise interactions [12] depending exclusively on the ratio d_1/d_2. As in our calculations, the scaling of the volume ensures a constant d_1/d_2 ratio, $A(d_1/d_2)$ is a constant and Eq. (1) can be used to evaluate the dislocation core energy $E(r_c)$.

The DFT calculations have been performed using the VASP package [33]. Following our previous study on MgO [29,30], we rely on PAW pseudopotentials and the Generalised Gradient Approximation (for further details the reader may refer to [29,30]). Whatever the investigated pressure, a single $2 \times 4 \times 6$ k-points mesh [34] was used to ensure a convergence of energies below 0.1 meV/atom. As already mentioned in the introduction part, we also rely on static calculations performed using the LAMMPS molecular dynamics package [35]. The empirical potential used in this case corresponds to a pairwise potential of the Buckingham form involving partial charges ($\pm 1.7e$) for Mg and O. We adopt the parameterization (B–G $\pm$ $1.7e$) proposed by Heinkelman et al. [36] with short-range interactions (*i.e.* <12 Å) computed between Mg–O and O–O. The long-range coulombic interactions were computed using an Ewald summation method [37] as implemented into the LAMMPS code. In Table 1, the unit cell parameters and the elastic constants of MgO have been calculated with the B–G $\pm$ $1.7e$ potential [36]. The cell parameters are consistent with DFT results in the whole pressure range. At 0 GPa of pressure, the elastic properties of MgO determined using the pairwise potential are close to the values obtained with the DFT (within about 10–15%). However, based on central interatomic force considerations, C_{ij} satisfy the Cauchy relation, C_{12}–$C_{44} = 2P$, in disagreement with either DFT calculations or experimental values [38]. The transferability of Heinkelman parameterization to the dislocation core structure calculations was therefore checked by the calculations of the Generalised Stacking Fault energy (GSF also called γ-surface) [39]. It turned out that the pairwise potential was able to accurately reproduced the energy landscape associated with the γ-surfaces as shown by the cross sections of the γ-surface (also called γ-lines) along $\frac{1}{2}\langle 1\,1\,0\rangle$ (Fig. 2) throughout the pressure range investigated (0–100 GPa) (calculations set-up for γ-surface calculations are described in [29,40]). At 0 GPa, the γ-lines are very well represented by the empirical potentials compared to those calculated in DFT (Fig. 2a). When pressure increases, the γ-lines calculated with the potential are under estimated with respect to those obtained in DFT calculations. However the potential mimics the inversion of the curves as observed in DFT. This result is surprisingly good when considering the simplicity of the potential without self consistent treatment of the charge. Based on γ-surfaces results the simulations performed with the Heinkelman parameterization are thus expected to capture properly the qualitative behaviour of the dislocations cores under high pressure.

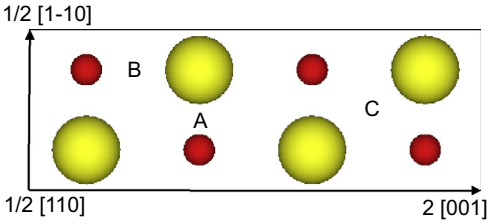


Fig. 1. MgO perfect crystal projected along the $\langle 1\,1\,0\rangle$ direction. Mg and O atoms correspond small and large spheres respectively. This basic block (see text for details) contains eight atoms. Labels A, B and C indicate the possible locations of the dislocation core, *i.e.* edge-A, edge-B and centre position, according to Ref. [21] terminology.

3. Results and discussion

Typical screw core structures with Burgers vector $\frac{1}{2}[1\,1\,0]$ extracted from the pairwise potentials calculations are shown Fig. 3 using the so-called differential displacement maps [41]. In Fig. 3, all atoms are displaced from their ideal crystal positions. However, as most of the displacements for a screw dislocation core are along the direction of the Burgers vector (*i.e.* [1 1 0] normal to the plane of the sheet in fig. 3), the dislocation core can only be visualized by plotting arrows between pairs of neighbouring atoms

Table 1
Lattice parameter a and elastic constant C_{ij} tensor for MgO determined from the parameterization of Heinkelman et al. [36]. Shear modulus μ is computed according to $\sqrt{C_{44}(C_{11}-C_{12})/2}$. All elastic quantities are given in GPa. First principles data [29,30] are given in brackets. γ^{max} correspond to the unstable stacking fault energy along a $\frac{1}{2}\langle 1\,1\,0\rangle$ shear in either $\{1\,1\,0\}$ or $\{0\,0\,1\}$ planes.

	0 GPa	30 GPa	60 GPa	100 GPa
a (Å)	4.22 (4.24)	4.05 (4.04)	3.94 (3.91)	3.83 (3.80)
C_{11}	281.5 (279)	466.7 (538)	633.0 (778)	838.2 (1088)
C_{12}	137.9 (93)	207.9 (138)	273.9 (179)	358.9 (230)
C_{44}	137.9 (146)	147.9 (170)	153.9 (187)	158.9 (202)
μ	99.5 (116.5)	138.4 (184.4)	166.2 (236.7)	195.2 (294.3)
γ^{max} ½ $\langle 1\,1\,0\rangle$ $\{1\,1\,0\}$ (J/m^2)	0.96 (1.05)	2.10 (2.45)	3.10 (3.72)	4.22 (5.28)
γ^{max} ½ $\langle 1\,1\,0\rangle$ $\{0\,0\,1\}$ (J/m^2)	2.22 (2.18)	2.90 (3.16)	3.16 (3.67)	3.31 (4.11)

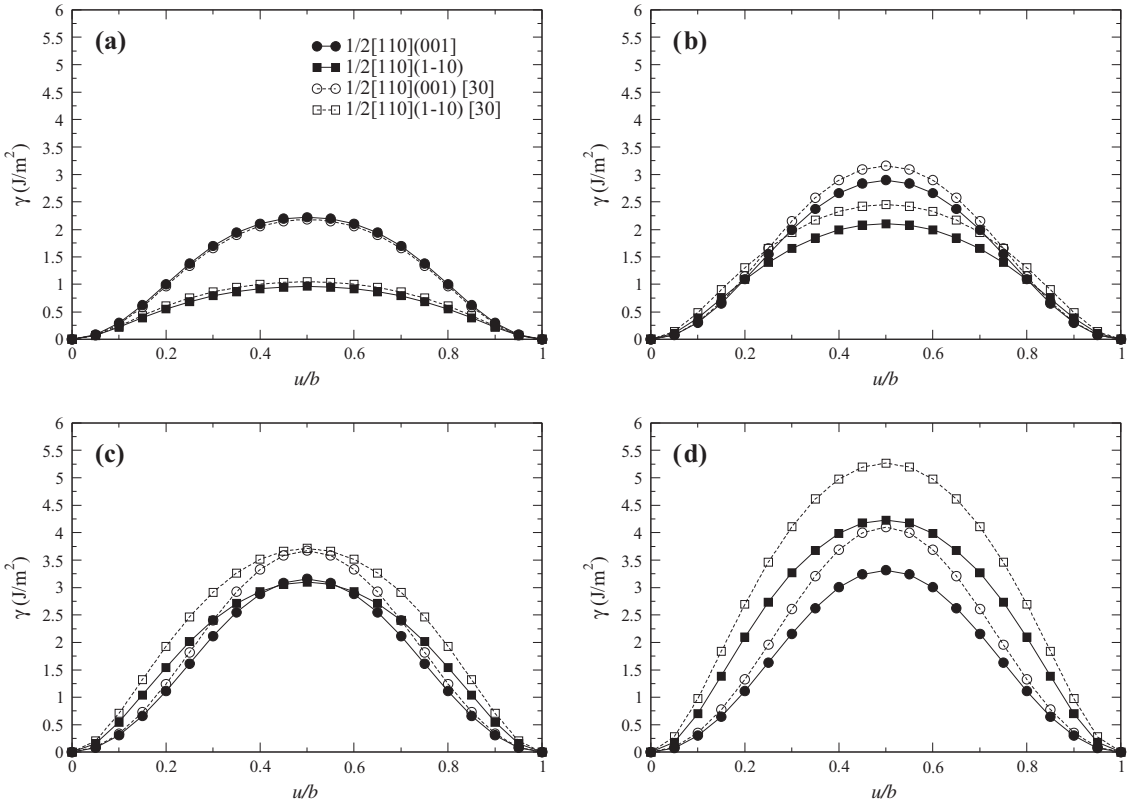


Fig. 2. Generalised Stacking Fault energy γ along $\frac{1}{2}\langle 1\,1\,0\rangle$ in $\{1\,1\,0\}$ (square) and $\{1\,0\,0\}$ (circle). The calculations have been done at 0 GPa (a), 30 GPa (b), 60 GPa (c) and 100 GPa (d). The differential evolution of γ energies between $(1\,-1\,0)$ and $(0\,0\,1)$ determined using the pairwise potential parameterization [36] (filled symbols) are in qualitative agreement with DFT results from Ref. [30] here shown as open symbols.

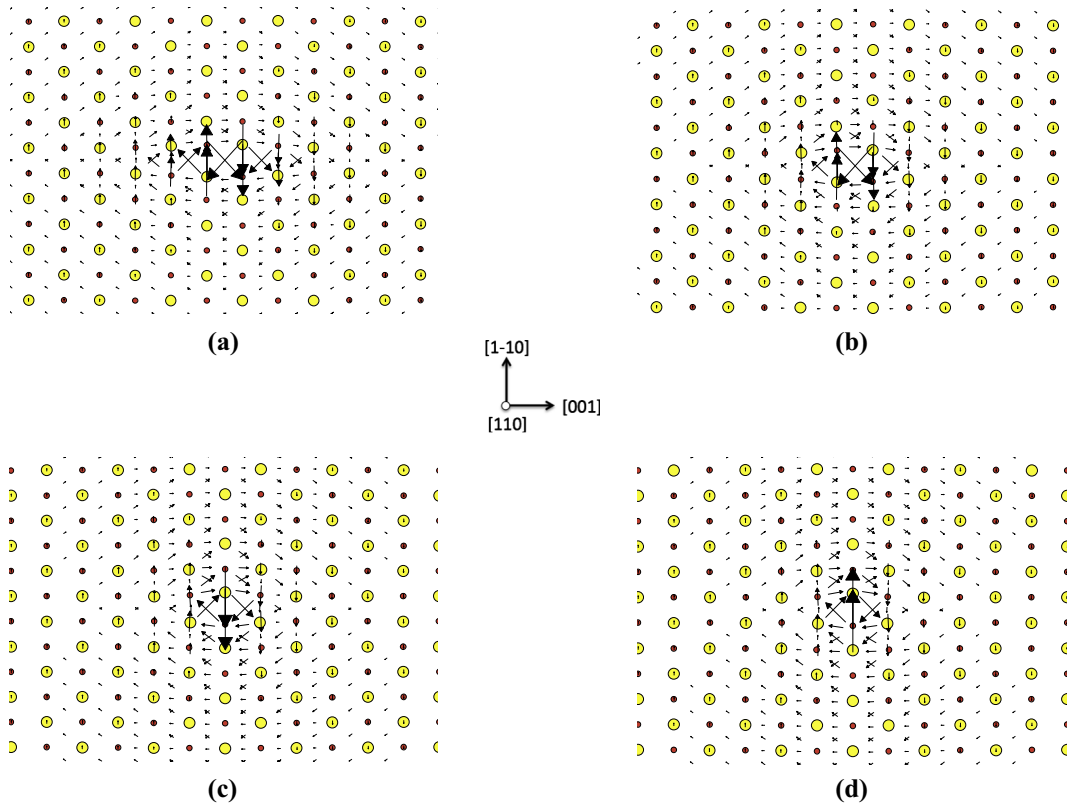


Fig. 3. Core configuration of the $\frac{1}{2}[1\,1\,0]$ screw dislocation for different pressure 0 GPa (a), 30 GPa (b), 60 GPa (c) and 100 GPa (d). The differential displacement arrows are plotted between the first and the second neighbours. The lengths of the arrows between neighbouring atoms are scaled to the relative displacement along the Burgers vector direction (perpendicular to the plane of representation).

with lengths proportional to the magnitudes of their relative displacements along [1 1 0] as compared to ideal positions in the perfect crystal. Thus Fig. 3 enables direct observations of the evolution of the core structure as a function of pressure. At low pressure (Fig. 3a), the core is fully spread in (1 −1 0) and extents over more than two unit cells. The increase of pressure leads to a decrease of core width associated with the simultaneous appearance of longer differential displacement arrows between pairs of atoms in (0 0 1). At 60 GPa, the core spreading in (1 −1 0) is already limited to a single unit cell along [0 0 1]. Moreover, most differential displacement arrows are now located in (0 0 1). DFT calculations lead to the same features. A comparison between empirical potential and DFT calculations is given in Fig. 4 where the atomic disregistries have been extracted from the atomic positions and plotted along either

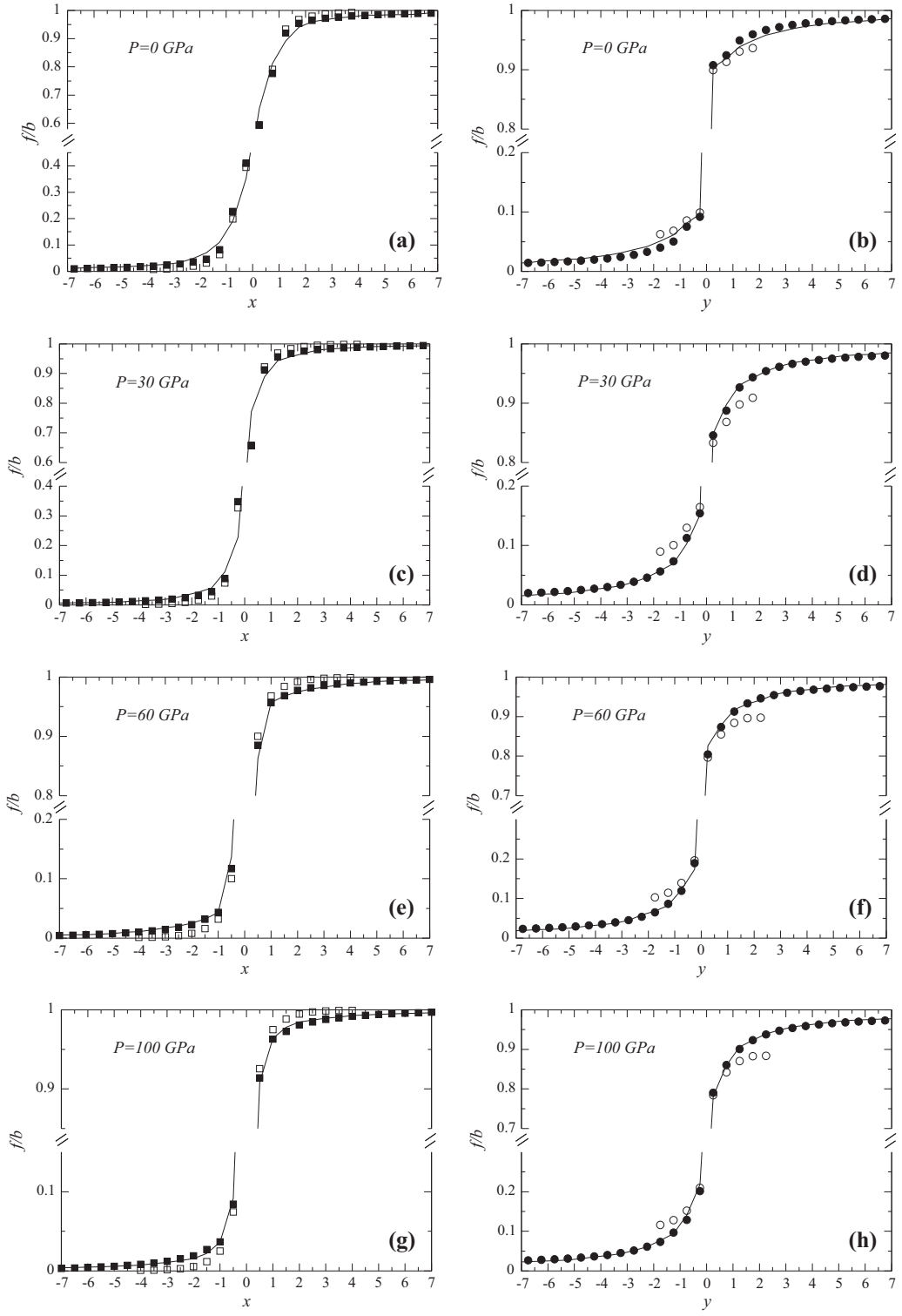


Fig. 4. Evolution of atomic disregistries as a function of pressure. Disregistries are plotted along [0 0 1] (*i.e.* x coordinate) in (1 −1 0) (left panel (a), (c), (e), (g)) and along [1 −1 0] (*i.e.* y coordinate) in (0 0 1) (right panel (b), (d), (f), (h). The pairwise potential data on the large cell ($n = 80$) are displayed as filled symbols and the DFT data (for a cell size $n = 8$) correspond to the open symbols. On all figures, the lines correspond to the solution of a continuum PN.

[001] or [1 −1 0] directions (*i.e.* within (1 −1 0) or (0 0 1) planes respectively). It is noticeable that the agreement between the two kinds of simulations is rather good, validating the choice of the pairwise potentials. Indeed, the atomic disregistries taken from both simulations are clearly overlapping except for the high pressure cells and only along [1 −1 0] in (0 0 1). This apparent discrepancy however may come from an artefact due to size effect. For high pressure calculation, where the spreading of the core is mostly found in (0 0 1) the small dimension of the cell used in DFT along the [1 −1 0] direction prevents a full spreading of the core. It is therefore impossible to reach a region of perfect crystal in between two dislocations along [1 −1 0], that was also the case of pairwise potential at high pressure and considering small volume (i.e. $n < 10$).

For comparison purpose between continuum modelling based on Peierls–Nabarro approach and atomistic calculations, continuum disregistries [30] have been plotted together with the current atomistic data in Fig. 4. It shows that continuum model and atomistic calculations are in perfect agreement. This demonstrates the accuracy of recent Peierls–Nabarro developments to predict core structures. Based on this comparison, we can further discuss the competition between elastic and inelastic forces involved in the dislocation core spreading. It should be reminded here that the pairwise potential used in this study does not enable to properly derivate the DFT set of elastic properties of MgO (Table 1). Thus, the core spreading agreement between the two methods strongly suggests that the dislocation core is mainly controlled by the inelastic force interaction captured by the γ-surface calculations. As already pointed out in [30], the core structure evolution found here can be viewed as the consequence of the evolution of the unstable stacking fault energies in {1 1 0} and {0 0 1} planes. Above 30 GPa, the lowest energy path along the ½⟨1 1 0⟩ shear direction belongs to {0 0 1}. As a consequence, the dislocation core tends to spread in {0 0 1} instead of {1 1 0}.

An interesting feature of the core corresponds to the exact stable position of the dislocation within the crystal lattice. Without any ambiguities, we can always define the dislocation centre as the position in the lattice for which the disregistry corresponds to $b/2$. It turns out that two distinct stable core centre positions can be identified depending on the applied pressure (see Figs. 3 and 5). The stable position of the dislocation core evolves from a centre site (labelled C on Fig. 1) at low pressure to an edge-A site (labelled A) at higher pressure. We use here the terminology introduced by Watson et al. [21] and recalled on Fig. 1. Our results at low pressure are consistent with those from Watson et al. [21] *i.e.* the ½⟨1 1 0⟩ screw core is stable at low pressure in a centre site (labelled C). Compared to an edge-A location, a centre position is often believed to be stable according to a short-range ion–ion interaction analysis [42]. Indeed, a screw dislocation in configuration edge-A brings in its core charged ions closer with a resulting bond length below 2/3 of their equilibrium distance (Fig. 5b). The short-range ion–ion repulsive forces should make therefore this configuration unfavourable to the profit of centre site (C). Nevertheless, the details of the core structure for a stable dislocation in a centre position show that similar configurations are arising (Fig. 5a) with oppositely charged ions on top of each other. Such unanticipated configuration for a core in centre site results here from the wide spreading of the core. It is worth noticing that a screw core lying in a (1 −1 0) glide plane is associated with a dilation state with an edge displacement component restricted to (1 −1 0) (Fig. 6a). The local edge displacements of the core thus allow to further accommodate the O–Mg distances in order to decrease the energy of the configuration. Therefore, one effect of pressure is to counteract this dilatation state. Under pressure, it is thus preferable to centre the core exactly in an edge-A location. This qualitative interpretation may also explain why whereas the core is spread in (0 0 1), the position edge-B could never been stabilized in our simulations. The change in stable position for the dislocation core structure may have further implications regarding the evolution of the Peierls potential of dislocation gliding in {1 1 0}. Indeed, based on our results, for a screw core gliding in {1 1 0}, the centre site should corresponds to the minimum of the Peierls valley at low pressure with a Peierls hill associated with

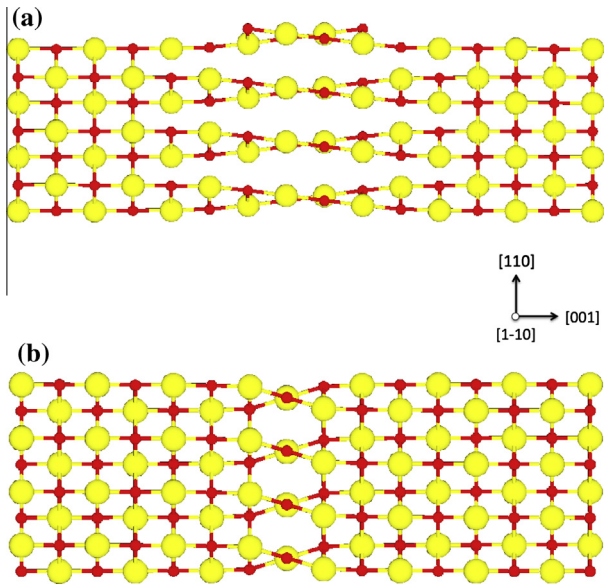


Fig. 5. View of the screw dislocation line lying on a (1 −1 0) glide plane. Only two layers of ions above and below the glide planes are displayed. (a) Typical configuration of a core located in the centre position (core calculated at 0 GPa). (b) Typical core configuration for a dislocation stabilized in the edge_A positions (calculations performed at a pressure of 100 GPa).

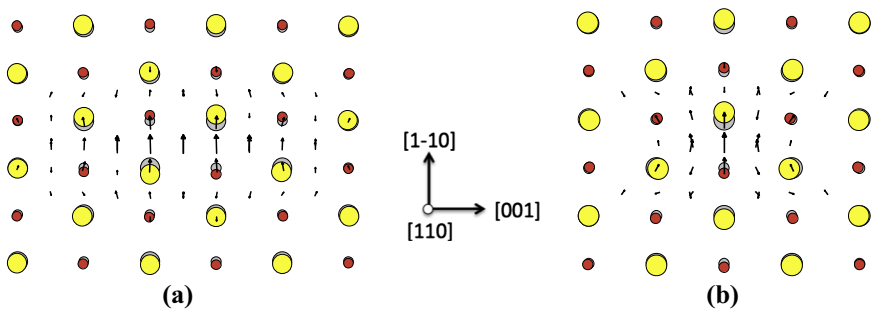


Fig. 6. Edge displacement inside the ½[1 1 0] screw dislocation core. (a) 0 GPa. (b) 100 GPa. Perfect atomic positions are displayed in grey to highlight the atomic displacements.

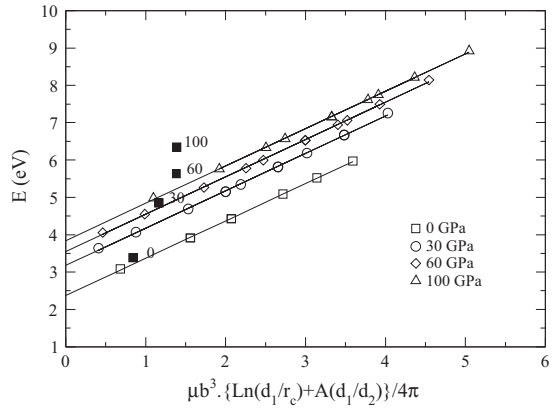


Fig. 7. Evolution of the total energy of the dislocation (elastic energy and core energy) obtained from the atomistic calculation as a function of the elastic energy of the dislocation only depending on the spacings into the quadrupole configurations (see Eq. (1)). Black symbols correspond to the DFT results.

the edge-A position. Under high pressure, the situation is thus expected to be reverse.

Finally, our calculations can be used to infer the core energy of the dislocation. Fig. 7 shows the evolution of the total energy of the dislocation (elastic energy and core energy) obtained from atomistic calculations as a function of the elastic part only (which depends on the dislocations spacing into the quadrupole configurations). As expected from Eq. (1), the strain energy of a dislocation within the quadrupolar arrangement scales with the equilibrium distance between pairs of dislocations with opposite sign. Eq. (1) and its representation on Fig. 7 can also be used to extract the core energy $E(r_c)$ of the dislocation as the y-intercept. As $E(r_c)$ depends on the choice of the core radius r_c, Fig. 7 has been plotted for a core radius of b. We found that $E(r_c = b)$ increases with pressure from 2.37 eV (under 0 GPa) to 3.84 eV (under 100 GPa). This reflects the core width evolution under pressure. Indeed, if now we adjust the core radius at each pressure in order to get the same core energy for all the pressure, and assuming that core radius at 0 GPa is still equal to b, we find that the pressure reduces the core width to 0.64b at 30 GPa, 0.55b at 60 GPa and 0.48b at 100 GPa. For the pairwise potential calculations, the fit of the cell energy according to Eq. (1) leads to the following shear modulus 95.6 GPa, 138.8 GPa, 170.3 GPa and 205.8 GPa for the simulations performed with a constant volume reflecting respectively 0, 30, 60 and 100 GPa of pressure. Shear moduli determined from the linear fit of Fig. 7 are thus comparable to those computed from the elastic constants (Table 1).

In Fig. 7, we also plot the results of the DFT calculations. As for the pairwise potential calculations, increasing pressure tends to increase the strain energy, except for the 100 GPa calculations where a strong overlap of the dislocations cores is observed. Focussing on the three first pressure investigated, it turns out that the DFT strain energies are systematically greater than those calculated with the pairwise potential. It is interesting to note that at low pressure, the difference between the two types of simulations is below 5% showing a remarkable agreement. We believe that a part of the discrepancy may originate from the large deviation of the elastic properties as pressure is increased.

4. Conclusion

Based on quadrupolar arrangement of periodic dislocations, our results confirm the major influence of pressure on the core spreading of the ½⟨1 1 0⟩ screw dislocation in MgO. We notice a remarkable agreement between atomistic core structures and continuum modelling based on PN approach. Within the framework of the PN model, a dislocation is spread continuously so as to minimize the energy of the core with respect to the GSF energies. Our results confirm that this assumption remains valid in MgO. Nevertheless, this study emphasizes the role of pressure by predicting, associated to different core spreading, a change in the stable position of the core with increasing pressure in the 100 GPa range. This new feature may have an influence on the Peierls potential in MgO under high pressures.

Acknowledgments

This work was supported by funding from the European Research Council under the Seventh Framework Programme (FP7), ERC Grant N°. 290424 – RheoMan. Computational resources have been provided by the CRI-Université de Lille 1. We thank two anonymous reviewers for their constructive comments that improved the clarity of the paper.

References

[1] M. Yamaguchi, V. Vitek, Core structure of nonscrew 1/2<1 1 1> dislocations on 1 1 0 planes in bcc crystals I. Core structure in an unstressed crystal, J. Phys. F Metal Phys. 3 (1973) 523–536.
[2] M.S. Duesbery, V. Vitek, Acta Mater. 46 (1998) 1481–1492.
[3] W. Xu, J.A. Moriarty, Comp. Mater. Sci. 9 (1998) 348–356.
[4] H. Koizumi, Y. Kamimura, T. Suzuki, Philos. Mag. A 80 (2000) 609–620.
[5] C. Woodward, S.I. Rao, Phys. Rev. Lett. 88 (2002) 216402.
[6] R. Groger, A.G. Bayley, V. Vitek, Plastic deformation of molybdenum and tungsten: I. Atomistic studies of the core structure and glide of 1/2<1 1 1> screw dislocations at 0 K, Acta Mater. 56 (2008) 5401.
[7] L. Pizzagalli, J.L. Demenet, J. Rabier, Phys. Rev. B 79 (2009) 045203.
[8] C. Woodward, Mater. Sci. Eng. A 400–401 (2005) 59–67.
[9] M. Ghazisaeidi, D.R. Trinkle, Acta Mater. 60 (2012) 1287–1292.
[10] W. Cai, Modelling dislocations using a periodic cell, in: S. Yip (Ed.), Handbook of Materials Modelling, Springer, Netherlands, 2005, pp. 813–826.
[11] S. Ismail-Beigi, T.A. Arias, Phys. Rev. Lett. 84 (2000) 1499–1502.
[12] G. Wang, A. Strachan, T. Cagin, W.A. Goddard III, Mater. Sci. Eng. A 309–310 (2001) 133–137.
[13] L. Ventelon, F. Willaime, J. Computer-Aided Mater. Des. 14 (2007) 85–94.
[14] E. Clouet, L. Ventelon, F. Willaime, Phys. Rev. Lett. 102 (2009) 055502.
[15] T.A. Arias, J.D. Joannopoulos, Phys. Rev. Lett. 73 (1994) 680–683.
[16] L. Pizzagalli, P. Beauchamp, Philos. Mag. Lett. 84 (2004) 729–736.
[17] C.H. Woo, M.P. Puls, J. Phys. C 9 (1976) L27–31.
[18] M.P. Puls, M.J. Norgett, J. Appl. Phys. 47 (1976) 466–477.
[19] C.H. Woo, M.P. Puls, Phil. Mag. 35 (1977) 727–756.
[20] C.H. Woo, M.P. Puls, Philos. Mag. 35 (1977) 1641–1652.
[21] G.W. Watson, E.T. Kelsey, S.C. Parker, Philos. Mag. A 79 (1999) 527–536.
[22] G.W. Watson, P.M. Oliver, S.C. Parker, Surf. Sci. 474 (2001) L185–L190.
[23] A.M. Walker, J.D. Gale, B. Slater, K. Wright, Phys. Chem. Chem. Phys. 7 (2005) 3227–3234.
[24] A.M. Walker, J.D. Gale, B. Slater, K. Wright, Phys. Chem. Chem. Phys. 7 (2005) 3235–3242.
[25] P. Hirel, M. Mrovec, C. Elsasser, Acta Mater. 60 (2012) 329–338.
[26] K.P. McKenna, J. Am. Chem. Soc. 135 (2013) 18859–18865.
[27] W. Cai, V.V. Bulatov, J.J. Chang, J. Li, S. S. Yip, Dislocation core effects on mobility, in: F.R.N. Nabarro, J.P. Hirth (Eds.), Dislocations in Solids, vol. 12, Elsevier, Amsterdam, 2004, pp. 1–80.
[28] C.R. Miranda, S. Scandolo, Comp. Phys. Comm. 169 (2005) 24–27.
[29] Ph. Carrez, D. Ferré, P. Cordier, Modelling Simul. Mater. Sci. Eng. 17 (2009) 035010.
[30] J. Amodeo, Ph. Carrez, P. Cordier, Philos. Mag. 92 (2012) 1523–1541.
[31] N. Lehto, S. Oberg, Phys. Rev. Lett. 80 (1998) 5568–5571.
[32] V.V. Bulatov, W. Cai, Computer simulations of dislocations, Oxford University Press, Oxford, 2006.
[33] G. Kresse, J. Hafner, Phys. Rev. B 47 (1993) 558–561.
[34] H.J. Monkhorst, J.D. Pack, Phys. Rev. B 13 (1976) 5188–5192.
[35] S. Plimpton, J. Comput. Phys. 117 (1995) 1–19.
[36] Heinkelman et al., Phys. Rev. B 72 (2005) (2005) 115437.
[37] P.J. In't Veld, A.E. Ismail, G.S. Grest, Application of Ewald summations to long-range dispersion forces, J. Chem. Phys. 127 (2007) 144711.
[38] B.B. Karki, L. Stixrude, S.J. Clark, M.C. Warren, G.J. Ackland, J. Crain, Am. Mineral. 82 (1997) 51–60.
[39] V. Vitek, Philos. Mag. 18 (1968) 773–786.
[40] K. Gouriet, Ph. Carrez, P. Cordier, Modelling Simul. Mater. Sci. Eng. 22 (2014) 025020.
[41] V. Vitek, R.C. Perrin, D.K. Bowen, Philos. Mag. 21 (1970) 1049–1073.
[42] J.P. Hirth, J. Lothe, Theory of Dislocations, second ed., John Wiley & Sons Inc, New York, 1982.